

Communication

Morphologically Controlled Synthesis of Cs₂SnCl₆ Perovskite Crystals and Their Photoluminescence Activity

Hongdan Zhang, Ludan Zhu, Jun Cheng, Long Chen, Chuanqi Liu and Shuanglong Yuan * 

Key Laboratory for Ultrafine Materials of Ministry of Education, School of Materials Science and Engineering, East China University of Science and Technology, Shanghai 200237, China; Y30160497@mail.ecust.edu.cn (H.Z.); Y30170516@mail.ecust.edu.cn (L.Z.); Y30170392@mail.ecust.edu.cn (J.C.); Y30180381@mail.ecust.edu.cn (L.C.); Y30180431@mail.ecust.edu.cn (C.L.)

* Correspondence: Shuanglong@ecust.edu.cn; Tel.: +86-21-64253395

Received: 17 April 2019; Accepted: 16 May 2019; Published: 18 May 2019



Abstract: The Cs₂SnX₆ perovskites have attracted much attention due to excellent optoelectronic properties and high stability. In the present work, we have focused on the morphology control and photoluminescence characteristics of the Cs₂SnCl₆ perovskite crystals. The synthesis process of the Cs₂SnCl₆ crystals includes two stages composed of the formation of initial crystals and the growth of Cs₂SnCl₆; the later originated from the oxidization of CsSnCl₃. This process has been confirmed by Scanning electron microscope (SEM) and X-rays diffraction (XRD). By controlling the concentration of the initial reactants and hydrochloric acid in the solution to change the supersaturation of the solution, different crystal morphologies, such as truncated octahedron, octahedron, hexapod, quasi-sphere, have been obtained. In relatively a low supersaturation solution, the amount of growth units dominates the crystal growth process to obtain the hexapod and self-assembly crystals. In contrast, in relatively high supersaturation solution, nucleation predominates to yield small size truncated octahedrons and near-spherical Cs₂SnCl₆ crystals. The synthesized Cs₂SnCl₆ crystals have shown a wide emission band peaking at 450 nm with full width at half maximum (FWHM) 63 nm due to the defects introduced by Sn²⁺. The photoluminescence intensities of crystals synthesized at various conditions exhibited considerable difference, which was about 60 times between the highest and the lowest.

Keywords: lead-free perovskite; Cs₂SnCl₆; crystal growth; photoluminescence

1. Introduction

In recent years, all-inorganic metal halide perovskite nanocrystals (generally CsPbX₃) have attracted scientific interest due to their attractive optoelectronic properties together with low cost and facile solution synthesis process, which have great potential in photovoltaic devices and light emitting devices [1–3]. In spite of their outstanding performance, all-inorganic lead halide perovskite still has to face the thorny issue that lead has intrinsic toxicity [4]. In view of non-toxic Sn²⁺ ions, tin (Sn)-based perovskite CsSnX₃ has been a very good alternative to be used in solar cells, infrared light emitting diodes and lasers [5–9]. Unfortunately, the CsSnX₃ perovskites still suffer from the oxidation of Sn²⁺ to more stable Sn⁴⁺, leading to a high sensitivity to the ambient atmosphere (oxygen, moisture, etc.) [5,6,10,11].

As a defect variant of the traditional cubic ABX₃ perovskite, Cs₂SnX₆ has a similar crystal structure with CsPbX₃. Cs₂SnX₆ is considerably stable to oxygen and moisture due to containing Sn⁴⁺ rather than Sn²⁺, therefore it is promising for large-scale production [12]. Recently, numerous publications

have reported their preparation methods and potential applications. Wang et al. [13] synthesized Cs_2SnI_6 nanocrystals and demonstrated that Cs_2SnI_6 based field effect transistors exhibit the property of P-type semiconductor with high hole mobility ($> 20\text{cm}^2/(\text{Vs})$). Dolzhenkov et al. [14] employed a thermal injection method to prepare Cs_2SnI_6 crystals with different sizes by controlling the reaction time and temperature. Kaltzoglou et al. [12] synthesized Cs_2SnCl_6 , Cs_2SnBr_6 , Cs_2SnI_6 and $\text{Cs}_2\text{SnI}_3\text{Br}_3$ crystals at a high temperature by using different solvents [15]. These crystals were employed as hole transport materials in dye-sensitized solar cell with the maximum power conversion efficiency of 4.23% under one solar irradiation [15]. Saparov et al. [4] obtained an n-type Cs_2SnCl_6 semiconductor film by annealing SnI_4 vapor to a glass substrate covered by a CsI film. Xiaofeng Qiu et al. [6] oxidized the CsSnI_3 film to Cs_2SnI_6 one as a light absorbing layer in a solar cell. In addition, Bi-doped Cs_2SnCl_6 has exhibited high efficient blue light emission originated from $[\text{Bi}_{\text{Sn}} + \text{V}_{\text{Cl}}]$ defect complex introduced by Bi^{3+} [16]. However, these studies have mainly focused on the particle size, optoelectronic characteristics and application of the Cs_2SnX_6 crystals in the field of optoelectronic devices. To our knowledge, rarely work has been done on their morphology control and photoluminescence characteristics.

Owing to the low solubility product constant of Cs_2SnCl_6 in aqueous hydrochloric acid, the reaction between cesium chloride and tin chloride is rapid, as a result, Cs_2SnCl_6 rapidly nucleates and grows. In this work, the growth process of Cs_2SnCl_6 crystals was studied by controlling the concentration of the reactants and hydrochloric acid. The Cs_2SnCl_6 crystals have shown interesting morphologies such as truncated octahedron, octahedron, hexapod and quasi-sphere. In addition, we have investigated the photoluminescence (PL) properties of Cs_2SnCl_6 crystals. They exhibited a similar wide emission band peaking at 450 nm with different intensities under 350 nm excitation.

2. Experiments

Tin (Sn, 99.9%, Aladdin, Shanghai, China), hydrochloric acid (HCl, 36-38%, Titan Technology Co., Ltd., Shanghai, China), cesium chloride (CsCl, 99.99%, Aladdin, Shanghai, China), deionized water (H_2O), absolute alcohol ($\text{C}_2\text{H}_6\text{O}$, Titan Technology Co., Ltd., Shanghai, China).

Firstly, tin powder was dissolved in a corresponding amount of HCl by a mole ratio of 1:4 to obtain a SnCl_2 hydrochloric acid solution. The corresponding amount of CsCl was added to a beaker, then deionized water and HCl (the amount of added HCl expressed as the concentration of hydrochloric acid in the solution) were added according to the calculated value and finally, 1.5 mmol SnCl_2 solution was added. The mixture was stirred in the air at room temperature for 7 h and then the precipitate was collected by centrifugation and washed with anhydrous ethanol. Finally, the product naturally dried in an ambient environment. Typically, 0.178 g Sn powders were dissolved in 0.125 mL HCl to prepare SnCl_2 solution, 0.505 g CsCl, 26.5 mL deionized water and additional 9 mL HCl were used to prepare the sample at the reaction condition of 0.042 mol/L reactants and 3 mol/L HCl.

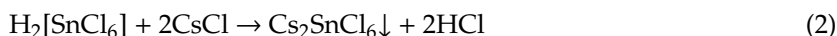
The morphology and particle size of the samples were measured with a Hitachi S-4800 scanning electron microscopy (SEM). The photoluminescence (PL) and photoluminescence excitation (PLE) spectra were determined by a Fluorolog-3-P UV-vis-NIR fluorescence spectrophotometer (Jobin Yvon, France). The absorption spectrum was obtained by a UV-2550 UV-VIS spectrophotometer (Shimadzu, Japan).

3. Result and Discussion

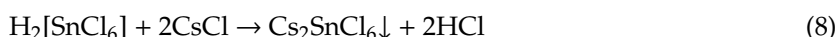
3.1. The Crystal Growth and Morphologies of the Cs_2SnCl_6 Crystals in Different Synthesis Conditions

In this work, SnCl_2 solution was prepared by dissolving Sn in HCl with a molar ratio of 1:4. In such a dissolution process, the oxygen from the air partially oxidized SnCl_2 to SnCl_4 in the presence of excessive HCl, leading to the coexistence of SnCl_2 and SnCl_4 in the obtained SnCl_2 solution (still expressed as SnCl_2 for convenience). Therefore, the formation process of the Cs_2SnCl_6 crystals includes two stages as follows:

Stage 1:



Stage 2:



In stage 2, an overall balanced reaction will be:



Such a process has been examined by XRD patterns of the samples at different reaction time (shown in Figure S1, see Supplementary materials). CsSnCl_3 and Cs_2SnCl_6 crystals firstly coexisted in the samples and then the diffraction peaks of CsSnCl_3 gradually disappeared and those of Cs_2SnCl_6 gradually increased with increasing the reaction time; finally, only the diffraction peaks of Cs_2SnCl_6 crystals were observed after a reaction time larger than 6 h. Therefore, the final crystal formation process consisted of two stages above mentioned. The first one was the fast nucleation and growth process of the initial Cs_2SnCl_6 and CsSnCl_3 crystals according to reactions (1)–(4), which were related to the concentration of HCl and initial reactants. The second one was the growth process of Cs_2SnCl_6 oxidized from CsSnCl_3 (see the Equations (5)–(8) about the oxidization and precipitation process) on the initial Cs_2SnCl_6 crystals during the first stage, that is, the initial Cs_2SnCl_6 crystals acted as the nuclei of the second growth stage, the growth rate also depended on the concentration of HCl and reactants. As the overall content of Cs_2SnCl_6 crystals was constant when the same initial reactants content had been employed, the ratio of Cs_2SnCl_6 crystals between the first and second stage remarkably impaired the crystal morphology.

Figure 1 presents the SEM images of the Cs_2SnCl_6 crystals (determined by XRD patterns in Figure S2 in Supplementary materials) synthesized by using different amounts of hydrochloric acid for 0.042 mol/L SnCl_2 solution. At 3 mol/L HCl, the complete octahedral crystals can be observed in Figure 1a. When the HCl concentration was increased to 5 mol/L, the crystals showed a uniform hexapod structure containing six thin and long carambola-like branches (Figure 1b). Interestingly, when the HCl concentration was increased to 9 and 10 mol/L, the hexapod crystals at different growth periods (Figure 1c,d), with an expanded volume and enlarged branches, were present clearly, in which some regular octahedrons with eight holes in eight faces of the octahedron can be seen apparently. These regular octahedrons were obviously composed of six small octahedral crystals growing along three orthogonal directions. The holes among these small octahedrons were gradually filled up into a complete smooth octahedron structure. To clearly be seen, the typical morphologies of the Cs_2SnCl_6 crystals at different HCl concentration have been shown in Figure 2 accompanied by the inset simulated diagram. For a face-centered cubic crystal [12], according to the law of Bravais [17], the normal sequence of crystal faces appearing is {111}, {100}, {110}. Therefore, the initial Cs_2SnCl_6 crystal nuclei are normal octahedral structure with eight {111} faces (Figure 2a). The growth process of the crystal changes from the octahedral spiral growth to the continuous growth of the branched crystal as the driving force (that is, the amount of the growth units Cs_2SnCl_6) increases [18], as a result, the morphologies of obtained Cs_2SnCl_6 crystals changed from the octahedron to the hexapod (Figure 2b–d) and then to the self-assembled bigger regular octahedron (Figure 2e,f). Such morphology changing process

is akin to the evolution of the Cu_2O crystal morphologies reported in the literature, which is called self-assembly [19].

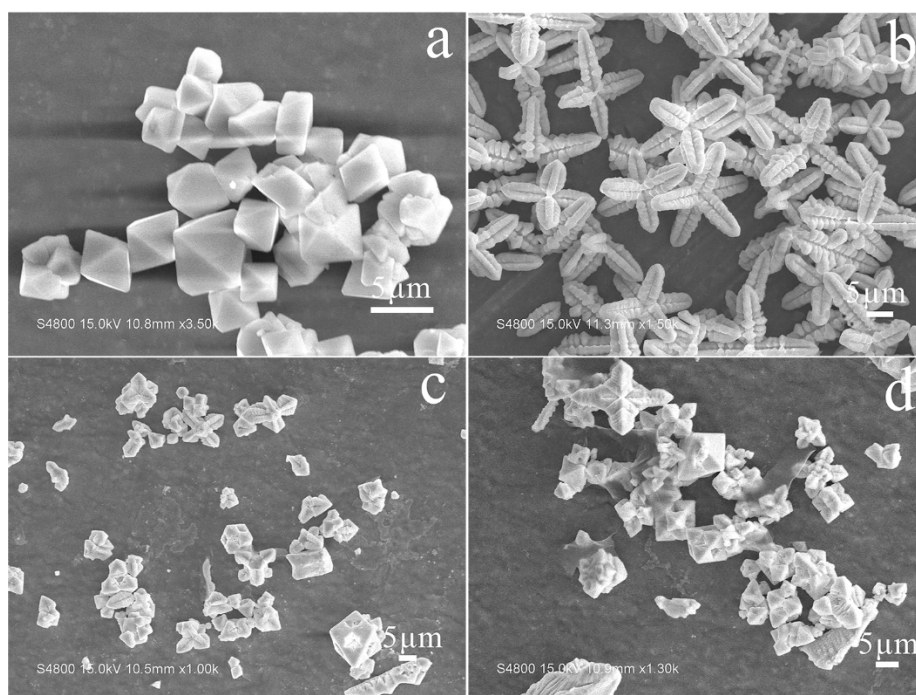


Figure 1. The SEM images of the Cs_2SnCl_6 crystals prepared with (a) 3 mol/L, (b) 5 mol/L, (c) 9 mol/L, (d) 10 mol/L HCl for 0.042 mol/L SnCl_2 solution.

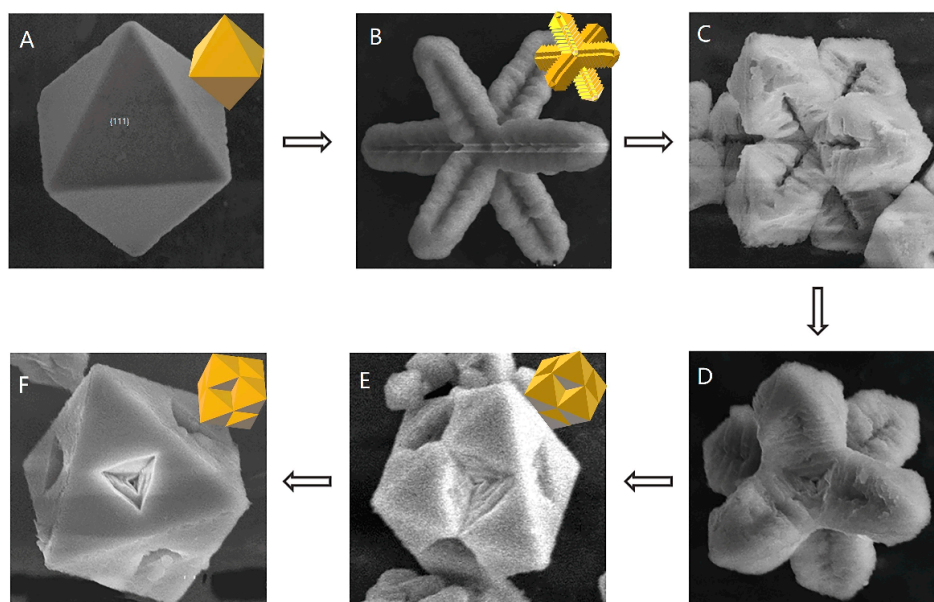


Figure 2. The self-assembly process of Cs_2SnCl_6 crystal (A) octahedron, (B–D) Hexapod, (E,F) Incomplete octahedron.

Figure 3 shows the morphologies of the Cs_2SnCl_6 crystals (determined by XRD, see Figure S3 in Supplementary materials) obtained by using different amounts of HCl for 0.083 mol/L SnCl_2 solution. At 3 mol/L HCl, there were some complete octahedrons (about 20 μm) accompanied by incomplete regular octahedrons (about 20–30 μm) with holes, which were similar to those in Figure 1. At 4 mol/L HCl, a uniform carambola-like structure with particle size about 20 μm was formed by rapidly growing incomplete octahedrons (Figure 3b). Six carambola-like particles may assemble to

a hexapod. By increasing the HCl concentration, the length of the hexapod branch decreased gradually leading to a smaller and smaller particle size. Finally, the morphologies varied from the hexapod to the truncated octahedron and then to the quasi-sphere.

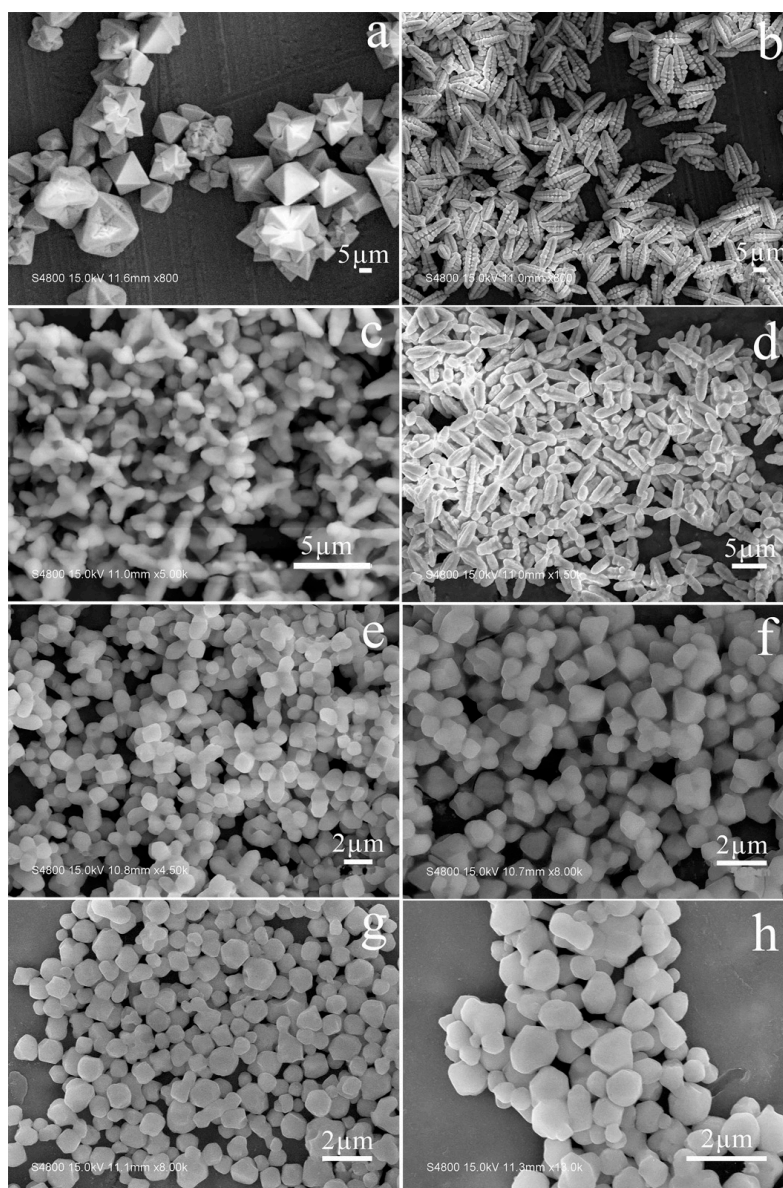


Figure 3. The SEM images of the Cs_2SnCl_6 crystals prepared by (a) 3 mol/L, (b) 4 mol/L, (c) 5 mol/L, (d) 6 mol/L, (e) 7 mol/L, (f) 8 mol/L, (g) 9 mol/L, (h) 10 mol/L HCl for 0.083 mol/L SnCl_2 .

These changes in morphology and size with increasing HCl content are related to the homogeneous nucleation and growth process of the crystals. The amount and morphology of the initial Cs_2SnCl_6 crystals depend on the supersaturation of the solution in the first stage of the initial crystal formation, the higher supersaturation results in larger amounts of nuclei as well as the amount of the initial Cs_2SnCl_6 crystals. As the initial Cs_2SnCl_6 crystals act as the nuclei of the second growth stage, the final particle size and morphology are related to the amount of Cs_2SnCl_6 oxidized from Cs_2SnCl_3 at stage 2 (see reactions (5–9)). This suggested that the ratio of Cs_2SnCl_6 crystals (defined as $R_{1/2}$) between the first and second stage plays a key role in the crystal morphology as mentioned above. During the two crystal formation stages, the final complete octahedron can be obtained if the amount of the initial Cs_2SnCl_6 crystals matches that during the second growth stage, in this case, we define $R_{1/2}$ as b

(means balance). $R_{1/2}$ larger than b means the larger amount of the initial crystals, contrarily the larger amount of Cs_2SnCl_6 produced in the second growth stage as the growth units. The crystals with the different dendritic degree form if $R_{1/2} > b$ because of insufficient Cs_2SnCl_6 growth units. Increasing the crystal growth units, the crystals grow from the dendritic to the self-assembly structure, and then to the complete smooth octahedron due to the continual growth of the growth units around the initial dendritic surface, in line with the morphology changing process in the case of the 0.042 mol/L SnCl_2 solution (Figure 2). In contrast, at the reactant concentration of 0.083 mol/L, the larger supersaturation led to more nuclei during the first stage, thus the growth units comparatively decreased, resulting in $R_{1/2} > b$. As a result, the morphologies of the Cs_2SnCl_6 crystals gradually changed from the fast-growing dendritic crystals to the fast-nucleating and slow-growing quasi-spherical particles, and the size decreased accordingly.

The difference of morphology changing between 0.042 and 0.083 mol/L reactants originated from the larger difference in the reactant concentration. Figure 4 presents the SEM images of the crystals with the different reactant concentrations at 5 mol/L HCl (For convenient comparison, the images of 0.042 and 0.083 mol/L have also shown in this figure). When the concentration of the reactants increased to 0.165 mol/L, the crystals exhibited a truncated octahedron structure with a particle size of only 1–2 μm as well as increasing the HCl concentration to 0.083 mol/L. At higher concentrations, nanosize Cs_2SnCl_6 crystals with impurities (the XRD patterns shown in Figure S4) were obtained (determined by Transmission electron microscope (TEM), shown in Figure S5 in Supplementary materials). According to the above discussion, the effect of the reaction conditions on the morphology of the Cs_2SnCl_6 crystals has been summarized in Figure 5 and Figure S6.

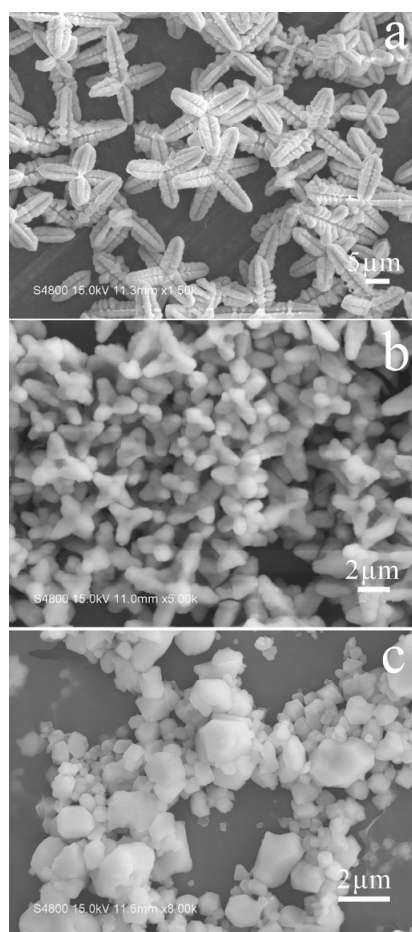


Figure 4. The SEM images of the Cs_2SnCl_6 crystals prepared at 5 mol/L HCl concentration for different SnCl_2 concentrations: (a) 0.042 mol/L, (b) 0.083 mol/L, (c) 0.167 mol/L.

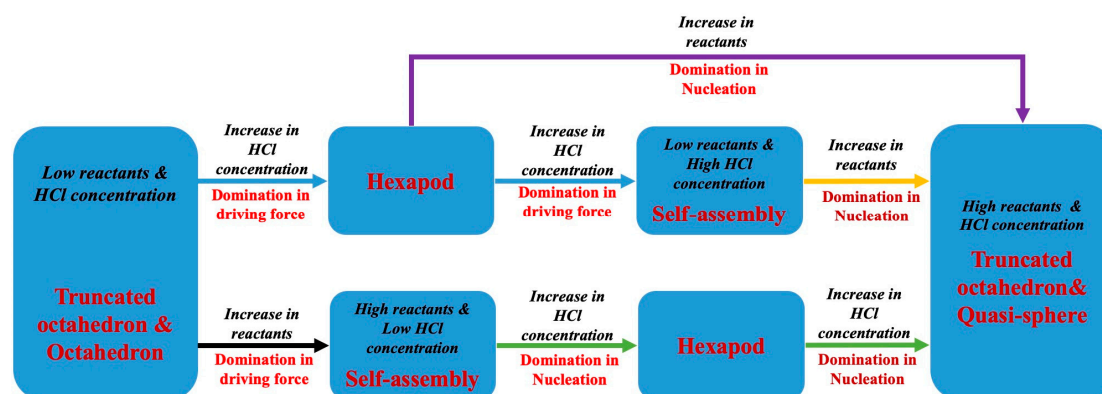


Figure 5. The summary flowchart of the crystal morphologies and synthesis conditions.

3.2. Photoluminescence Characteristics

As a kind of perovskite, Cs_2SnCl_6 also exhibited highly efficient blue light emission originated from $[\text{Bi}_{\text{Sn}} + \text{V}_{\text{Cl}}]$ defect complex introduced by Bi^{3+} [16], however, no report about the photoluminescence of the Cs_2SnCl_6 crystal without dopants has been published except for the recent work [20] to the best of our knowledge. Figure 6a shows the PL spectra of the crystals prepared at 0.083 mol/L SnCl_2 solution and different HCl concentrations under 350 nm excitation; the PLE and PL spectra of the crystals in Figure 3g are shown in Figure 6b. The PL spectrum of the Cs_2SnCl_6 crystals has a wide emission band peaking at 450 nm with FWHM 63 nm and a large Stokes shift about 100 nm. The absorption spectra (Figure S7) have shown weak and wide absorption band about 350 nm when the crystals exhibited strong photoluminescence characteristics, reversely, this absorption band could not be distinguished from the non-photoluminescence crystals. This is similar to the literature [16], indicating that such emission spectra also originate from some kinds of defects, which are $\text{V}_{\text{Sn(IV)}}$ and V_{Cl} due to Sn^{2+} in the crystals (see XPS spectra in Figure S8). It suggests the existence of the characteristic $3d_{3/2}$ (495.7 eV) and $3d_{5/2}$ (487.2 eV) peaks of Sn^{2+} in addition to Sn^{4+} $3d_{3/2}$ (496.1 eV) and $3d_{5/2}$ (487.6 eV) [16,19]. The intensity of the PL emission peak depends on the number of defects in the crystals, and that of high purity and uniform crystals is relatively weaker [21,22], the highest one is 60 times larger than the lowest one as shown in Figure 6a. However, the relationship between the photoluminescence intensity and the crystal morphology is still irregular. Besides, the huge difference in photoluminescence intensity is significantly associated with the number of defects owing to the different reaction condition. These have been discussed in detail in our recent work [22].

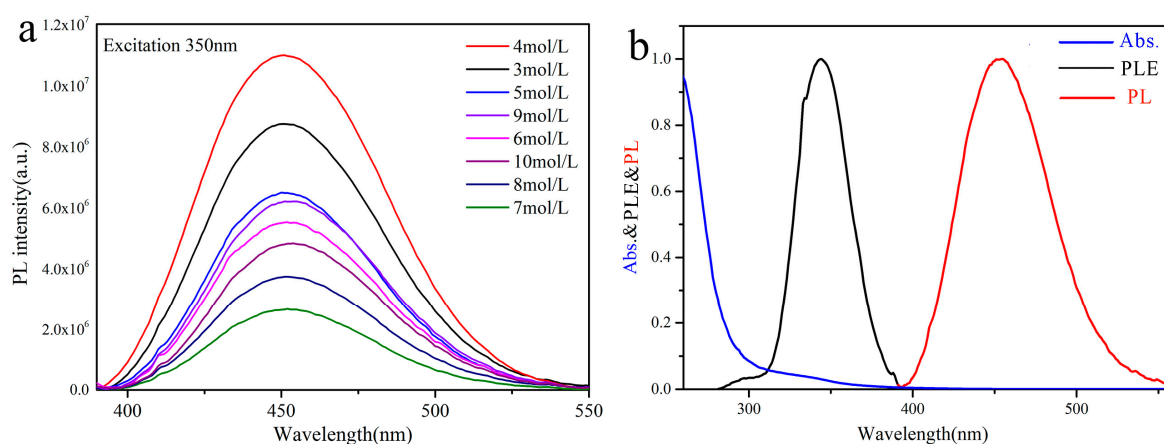


Figure 6. (a) The PL spectra of the Cs_2SnCl_6 crystals in Figure 3. (b) The absorption, PL and PLE spectra of the Cs_2SnCl_6 crystals in Figure 3g.

4. Conclusions

In summary, the different crystal morphologies of Cs_2SnCl_6 , such as truncated octahedron, octahedron, hexapod, quasi-sphere, have been obtained by controlling the initial reactants and HCl concentration in the solution. The amount of crystal nucleation and growth units increases as increasing the initial reactants HCl concentration. When the amount of nucleation is more than the growth units, nucleation controls the crystal growth to obtain crystals with different dendrites. Conversely, when the number of growth units is larger, the driving force controls the crystal growth to obtain the hexapod and self-assembled crystals. Under 350 nm excitation, the Cs_2SnCl_6 crystals exhibit a wide emission band peaking at 450 nm with an FWHM of 63 nm and a large Stokes shift of 100 nm. Due to the influence of the defects number, the highest one is 60 times larger than the lowest one.

Supplementary Materials: The following are available online at <http://www.mdpi.com/2073-4352/9/5/258/s1>, Figure S1: XRD patterns of the Cs_2SnCl_6 crystals prepared at different time, with a hydrochloric acid concentration of 5 mol/L and an SnCl_2 concentration of 0.083 mol/L, Figure S2: XRD patterns of the Cs_2SnCl_6 crystals synthesized at different HCl concentrations (3, 5, 9, 10 mol/L) in the aqueous solution with SnCl_2 concentration 0.042 mol/L, Figure S3: XRD patterns of the Cs_2SnCl_6 crystals synthesized at different HCl concentrations in the aqueous solution with SnCl_2 concentration 0.083 mol/L, Figure S4: XRD patterns of the Cs_2SnCl_6 crystals synthesized at different SnCl_2 concentration in the aqueous solution with a hydrochloric acid concentration of 5 mol/L, Figure S5: HR-TEM images of the Cs_2SnCl_6 crystals prepared at normal temperature in the aqueous solution with a hydrochloric acid concentration of 5 mol/L and a SnCl_2 concentration of (a, b) 0.208 mol/L, (c, d) 0.250 mol/L, Figure S6: Summary of crystal morphology and synthesis conditions, Figure S7: UV-vis absorption spectroscopy of the Cs_2SnCl_6 crystals prepared with 0.083 mol/mL SnCl_2 and different concentration of HCl. The illustration is a partial magnification between 300–400 nm, Figure S8: (a) XPS survey spectrum of Cs_2SnCl_6 crystals prepared with 0.083 mol/mL SnCl_2 and different concentration of HCl. (b) High-resolution XPS spectra and peak fitting for Sn 3d.

Author Contributions: Investigation, H.Z. and L.Z.; Resource, J.C., L.C. and C.L.; Writing—Original Draft Preparation, H.Z.; Writing—Review and Editing, S.Y.

Conflicts of Interest: We declare that we have no financial and personal relationships with other people or organizations that can inappropriately influence our work, there is no professional or other personal interest of any nature or kind in any product, service and/or company that could be construed as influencing the position presented in, or the review of, the manuscript entitled.

References

1. Palazon, F.; Di Stasio, F.; Akkerman, Q.A.; Krahne, R.; Prato, M.; Manna, L. Polymer-free Films of Inorganic Halide Perovskite Nanocrystals as UV-to-White Color-conversion Layers in LEDs. *Chem. Mater.* **2016**, *28*, 2902–2906. [CrossRef]
2. Wang, Y.; Li, X.; Song, J.; Xiao, L.; Zeng, H.; Sun, H. All-inorganic Colloidal Perovskite Quantum Dots: A New Class of Lasing Materials with Favorable Characteristics. *Adv. Mater.* **2015**, *27*, 7101–7108. [CrossRef]
3. Ramasamy, P.; Lim, D.H.; Kim, B.; Lee, S.H.; Lee, M.S.; Lee, J.S. All-inorganic cesium lead halide perovskite nanocrystals for photodetector applications. *Chem. Commun.* **2016**, *52*, 2067–2070. [CrossRef] [PubMed]
4. Saporov, B.; Sun, J.P.; Meng, W.; Xiao, Z.; Duan, H.S.; Gunawan, O.; Shin, D.; Hill, I.G.; Yan, Y.; Mitzi, D.B. Thin-film Deposition and Characterization of a Sn-deficient Perovskite Derivative Cs_2SnI_6 . *Chem. Mater.* **2016**, *28*, 2315–2322. [CrossRef]
5. Lee, B.; Stoumpos, C.C.; Zhou, N.; Hao, F.; Malliakas, C.; Yeh, C.Y.; Marks, T.J.; Kanatzidis, M.G.; Chang, R.P. Air-stable Molecular Semiconducting Iodosalts for Solar Cell Applications: Cs_2SnI_6 as a Hole Conductor. *J. Am. Chem. Soc.* **2014**, *136*, 15379–15385. [CrossRef]
6. Qiu, X.; Cao, B.; Yuan, S.; Chen, X.; Qiu, Z.; Jiang, Y.; Ye, Q.; Wang, H.; Zeng, H.; Liu, J.; et al. From Unstable CsSnI_3 to Air-stable Cs_2SnI_6 : A Lead-free Perovskite Solar Cell Light Absorber with Bandgap of 1.48eV and High Absorption Coefficient. *Sol. Energ. Mat. Sol. C.* **2017**, *159*, 227–234. [CrossRef]
7. Noel, N.K.; Stranks, S.D.; Abate, A.; Wehrenfennig, C.; Guarnera, S.; Haghighirad, A.A.; Sadhanala, A.; Eperon, G.E.; Pathak, S.K.; Johnston, M.B.; et al. Lead-free Organic–inorganic Tin Halide Perovskites for Photovoltaic Applications. *Energ. Environ. Sci.* **2014**, *7*, 3061–3068. [CrossRef]
8. Xing, G.; Kumar, M.H.; Chong, W.K.; Liu, X.; Cai, Y.; Ding, H.; Asta, M.; Gratzel, M.; Mhaisalkar, S.; Mathews, N.; et al. Solution-processed Tin-based Perovskite for Near-infrared Lasing. *Adv. Mater.* **2016**, *28*, 8191–8196. [CrossRef]

9. Lai, M.L.; Tay, T.Y.; Sadhanala, A.; Dutton, S.E.; Li, G.; Friend, R.H.; Tan, Z.K. Tunable Near-infrared Luminescence in Tin Halide Perovskite Devices. *J. Phys. Chem. Lett.* **2016**, *7*, 2653–2658. [[CrossRef](#)]
10. Qiu, X.; Jiang, Y.; Zhang, H.; Qiu, Z.; Yuan, S.; Wang, P.; Cao, B. Lead-free Mesoscopic Cs₂SnI₆ Perovskite Solar Cells Using Different Nanostructured ZnO Nanorods As Electron Transport Layers. *Phys. Status Solidi-RRL.* **2016**, *10*, 587–591. [[CrossRef](#)]
11. Xiao, Z.; Zhou, Y.; Hosono, H.; Kamiya, T. Intrinsic Defects in a Photovoltaic Perovskite Variant Cs₂SnI₆. *Phys. Chem. Chem. Phys.* **2015**, *17*, 18900–18903. [[CrossRef](#)] [[PubMed](#)]
12. Kaltzoglou, A.; Antoniadou, M.; Kontos, A.G.; Stoumpos, C.C.; Perganti, D.; Siranidi, E.; Raptis, V.; Trohidou, K.; Psycharis, V.; Kanatzidis, M.G.; et al. Optical-vibrational Properties of the Cs₂SnX₆ (X = Cl, Br, I) Defect Perovskites and Hole-transport Efficiency in Dye-sensitized Solar Cells. *J. Phys. Chem. C* **2016**, *120*, 11777–11785. [[CrossRef](#)]
13. Wang, A.; Yan, X.; Zhang, M.; Sun, S.; Yang, M.; Shen, W.; Pan, X.; Wang, P.; Deng, Z. Controlled Synthesis of Lead-free and Stable Perovskite Derivative Cs₂SnI₆ Nanocrystals via a Facile Hot-injection Process. *Chem. Mater.* **2016**, *28*, 8132–8140. [[CrossRef](#)]
14. Dolzhenkov, D.S.; Wang, C.; Xu, Y.; Kanatzidis, M.G.; Weiss, E.A. Ligand-free, Quantum-confined Cs₂SnI₆ Perovskite Nanocrystals. *Chem. Mater.* **2017**, *29*, 7901–7907. [[CrossRef](#)]
15. Kaltzoglou, A.; Antoniadou, M.; Perganti, D.; Siranidi, E.; Raptis, V.; Trohidou, K.; Psycharis, V.; Kontos, A.G.; Falaras, P. Mixed-halide Cs₂SnI₃Br₃ Perovskite as Low Resistance Hole-transporting Material in Dye-sensitized Solar Cells. *Electrochim. Acta* **2015**, *184*, 466–474. [[CrossRef](#)]
16. Tan, Z.; Li, J.; Zhang, C.; Li, Z.; Hu, Q.; Xiao, Z.; Kamiya, T.; Hosono, H.; Niu, G.; Lifshitz, E.; et al. Highly Efficient Blue-emitting Bi-doped Cs₂SnCl₆ Perovskite Variant: Photoluminescence Induced by Impurity Doping. *Adv. Funct. Mater.* **2018**, *28*, 1801131. [[CrossRef](#)]
17. Donnay, D.J.D.; Harker, D. A New Law of Crystal Morphology Extending the Law of Bravais. *Am. Mineral.* **1937**, *22*, 446–467.
18. Sunagawa, I. Growth and Morphology of Crystals. *Forma-Tokyo* **1999**, *14*, 147–166.
19. Giuseppe, A.; Nuccio, B.; John, R.F.; Antta, F.; Giovanna, I.; Giovanni, P.; Maria, V.R. Mössbauer, Far-infrared, and XPS Investigations of SnCl₂ and SnCl₄ Introduced in Polyconjugated Monosubstituted Acetylene Matrices. *Appl. Spectrosc.* **1995**, *49*, 237–240.
20. Zhang, H.; Zhu, L.; Cheng, J.; Chen, L.; Liu, C.; Yuan, S. Photoluminescence Characteristics of Sn²⁺ and Ce³⁺-doped Cs₂SnCl₆ Double-perovskite Crystals. *Materials* **2019**, *12*, 1501. [[CrossRef](#)] [[PubMed](#)]
21. Ho, J.Y.; Huang, M.H. Synthesis of Submicrometer-sized Cu₂O Crystals with Morphological Evolution from Cubic to Hexapod Structures and Their Comparative Photocatalytic Activity. *J. Phys. Chem. C* **2009**, *113*, 14159–14164. [[CrossRef](#)]
22. Zhang, B.; Guo, F.; Yang, L.; Jia, X.; Liu, B.; Xie, Z.; Chen, D.; Lu, H.; Zhang, R.; Zheng, Y. Shape-evolution Control of Hybrid Perovskite CH₃NH₃PbI₃ Crystals via Solvothermal Synthesis. *J. Cryst. Growth* **2017**, *459*, 167–172. [[CrossRef](#)]

